Vinculin is required for neuronal mechanosensing but not for axon outgrowth

DOI:
10.1016/j.yexcr.2021.112805

Document Version
Accepted author manuscript

Journal Pre-proof

Vinculin is required for neuronal mechanosensing but not for axon outgrowth

De-Yao Wang, Cristina Melero, Ashwaq Albaraky, Paul Atherton, Karin A. Jansen, Andrea Dimitracopoulos, Federico Dajas-Bailador, Adam Reid, Kristian Franze, Christoph Ballestrem

PII: S0014-4827(21)00358-X

DOI: https://doi.org/10.1016/j.yexcr.2021.112805

Reference: YEXCR 112805

To appear in: *Experimental Cell Research*

Received Date: 25 February 2021

Revised Date: 19 July 2021

Accepted Date: 21 August 2021

Please cite this article as: D.-Y. Wang, C. Melero, A. Albaraky, P. Atherton, K.A. Jansen, A. Dimitracopoulos, F. Dajas-Bailador, A. Reid, K. Franze, C. Ballestrem, Vinculin is required for neuronal mechanosensing but not for axon outgrowth, *Experimental Cell Research*, https://doi.org/10.1016/j.yexcr.2021.112805.

De-Yao Wang: Conceptualisation, Investigation, Formal analysis, Funding acquisition, Writing – original draft.; **Cristina Melero:** Investigation, Formal analysis, Methodology, Validation, Writing Review and editing, Visualisation; **Karen Jansen:** Investigation, Validation, Writing – Review & Editing, Visualisation; **Ashwaq Albaraky:** Investigation, Formal analysis; **Paul Atherton:** Writing - original draft & review & editing, Formal analysis, Methodology; **Federico Dajas-Bailador:** Conceptionalisation, Methodology and Writing-review; **Andrea Dimitracopoulos:** formal analysis and validation; **Adam Reid:** writing – review; **Kristian Franze** and **Christoph Ballestrem:** Conceptionalisation, Funding acquisition, Project Administration, Supervision, Writing-original draft & Data Curation.

Title: **Vinculin is required for neuronal mechanosensing but not for axon outgrowth**

Authors and Affiliations: De-Yao Wang*[1], Cristina Melero*[1], Ashwaq Albaraky[1], Paul Atherton[1,6], Karin A. Jansen[1], Andrea Dimitracopoulos[2], Federico Dajas-Bailador[3], Adam Reid[4,5], Kristian Franze[2,6,7] and Christoph Ballestrem†[1].

1. Division of Cell Matrix Biology and Regenerative Medicine, School of Biological Sciences, Faculty of Biology, Medicine and Health. The University of Manchester, Oxford Road. Manchester M13 9PT, UK

2. Department of Physiology, Development and Neuroscience. University of Cambridge, Downing Street. Cambridge CB2 3DY, UK

3. School of Life Sciences, University of Nottingham, NG7 2UH, UK

4. Blond McIndoe Laboratories, Division of Cell Matrix Biology and Regenerative Medicine, School of Biological Sciences, Faculty of Biology, Medicine and Health. The University of Manchester, Manchester Academic Health Science Centre. Manchester M13 9PT, UK

5. Department of Plastic Surgery & Nurns, Wythenshawe Hospital, Manchester University NHS Foundation Trust. Manchester Academic Health Science Centre. Manchester M23 9LT, UK

6. Institute of Medical Physics, Friedrich-Alexander University Erlangen-Nuremberg, 91052 Erlangen, Germany

7. Max-Planck-Zentrum für Physik und Medizin, 91054 Erlangen, Germany

* indicates equal contribution of authors

† indicates corresponding author: christoph.ballestrem@manchester.ac.uk

Conflict of interest: the authors have expressed no conflict of interest

Running head: Vinculin regulates neuronal mechanosensing

Abbreviations:

CAD: catecholaminergic-a differentiated

CNS: central nervous system

CPNs: cortical primary neurons

ECM: extracellular matrix

FA/s: focal adhesion/s

FACS: fluorescence-activated cell sorting

FAK: focal adhesion kinase

FAK[i]: focal adhesion kinase inhibitor

FN: fibronectin

LN: laminin

PAA: polyacrylamide gels

PC/s: point contact/s

PLL: poly-L-lysine

Abstract:

Integrin receptors are transmembrane proteins that bind to the extracellular matrix (ECM). In most animal cell types integrins cluster together with adaptor proteins at focal adhesions that sense and respond to external mechanical signals. In the central nervous system (CNS), ECM proteins are sparsely distributed, the tissue is comparatively soft and neurons do not form focal adhesions. Thus, how neurons sense tissue stiffness is currently poorly understood. Here, we found that integrins and the integrin-associated proteins talin and focal adhesion kinase (FAK) are required for the outgrowth of neuronal processes. Vinculin, however, whilst not required for neurite outgrowth was a key regulator of integrin-mediated mechanosensing of neurons. During growth, growth cones of axons of CNS derived cells exerted dynamic stresses of around 10-12 Pa on their environment, and axons grew significantly longer on soft (0.4 kPa) compared to stiff (8 kPa) substrates. Depletion of vinculin blocked this ability of growth cones to distinguish between soft and stiff substrates. These data suggest that vinculin in neurons acts as a key mechanosensor, involved in the regulation of growth cone motility.

Introduction:

During development and regeneration, neurons extend axons that navigate through a highly complex environment to connect with their target tissue. Failure to do so has detrimental consequences for the whole organism. Axon outgrowth is largely driven by growth cones, actin-rich structures localised at the tip of growing axons (Myers et al., 2011). For growth cone advance, as well as non-neuronal cell migration (Meili et al., 2010; Vicente-Manzanares et al., 2009), molecular forces are vital (Myers et al., 2011). These forces are generated by actomyosin, which is linked to the extracellular environment by specific anchoring points.

Such anchoring points consist of multimolecular adhesion complexes that physically transmit mechanical information from the outer environment to the inside of cells (outside-in) as well as from the contractile cytoskeleton to the outside of the cell (inside-out). In most animal tissue cells, these adhesion complexes are large (up to around 5-7 μm in length) structures named focal adhesions (FAs). Neuronal cells, in contrast, have much smaller (around 1-2 μm) adhesion complexes called point contacts (PCs) (Myers et al., 2011). While the FA machinery plays a major role in sensing biochemical (Hynes, 2002) and mechanical (Jansen et al., 2017) ECM properties, it is unclear whether neuronal PCs contribute to ECM sensing in a similar manner.

It is currently thought that PCs contribute to growth cone protrusion (Lin et al., 1996; Paul C. Bridgman, 2001) through a combination of actin polymerisation and actomyosin tension that provide protrusive and traction forces required for the advance of the growth cone (Franze, 2020). Such mechanisms may also be important in guiding axon outgrowth in response to ECM-mediated guidance cues (Kerstein et al., 2015). Recent *in vivo* data showed that not only the type of ECM, but also local tissue stiffness regulates axon pathfinding in the developing brain (Koser et al., 2016; Thompson et al., 2019), indicating that PCs and associated signals may also be involved in mechanosensing.

Both PCs and FAs consist of transmembrane receptors (integrins) that indirectly connect the intracellular cytoskeleton to the outside environment, i.e., the extracellular matrix (Giannone et al., 2009). Core FA proteins, including talin, vinculin, FAK, and paxillin (Horton et al., 2015), are also present in neurons (C.O. Arregui, 1994; Gomez et al., 1996; Renaudin et al., 1999). Talin and vinculin are key adapter proteins that link integrins to the actin cytoskeleton (Atherton et al., 2020; Atherton et al., 2015). Talin binds directly to integrins and a talin-vinculin complex forms the link to filamentous actin (F-actin) (Critchley, 2004; Ziegler et al.,

2008). In FAs of non-neuronal cells, this connection with F-actin provides mechanical force transmission to facilitate mechanical feedback through signalling proteins such as FAK and paxillin (Stutchbury et al., 2017). Whether these proteins function similarly in PCs to regulate neuronal mechanosensing is currently unclear. FAK and paxillin are known to modulate axon outgrowth (Myers and Gomez, 2011; Navarro and Rico, 2014; Robles and Gomez, 2006; Woo et al., 2009), but whether talin and vinculin play similar roles remains to be elucidated.

Whilst the basic structure of PCs and FAs show a number of similarities, there are also important differences. In particular, FAs bear significantly larger forces than PCs (Athamneh and Suter, 2015). Since forces can contribute to the activation of proteins such as talin and vinculin (Atherton et al., 2015; Goult et al., 2018; Jansen et al., 2017), changes of force regimes may have a large impact on signalling events and mechanisms that regulate cell motility.

In the present study, we assessed the contribution of regulatory proteins that control cell-matrix adhesion to axon growth and mechanosensing. Using photoactivatable probes, we visualised cell-matrix adhesions in growth cones at the base of filopodia where traction forces are generated. We found that, whilst talin and FAK are critical for ECM-mediated axon outgrowth; deletion of vinculin had no effect on axon growth. To test how PCs contribute to neuronal mechanosensing, we cultured neurons on ECM-coated hydrogels with different stiffnesses. CNS-derived neurons sensed differences between soft and stiff substrates. The ability of neurons to determine differences in substrate stiffness depended on vinculin. Our results suggest that, despite a different force regime, neuronal PCs function similarly to FAs in non-neuronal cells and are crucial for growth cone motility and mechanosensing.

Results:

PCs localize to the base of growth cone filopodia.

Some experiments, and particularly fluorescence live cell imaging, are inherently difficult to perform in cortical primary neurons (CPNs). CPNs are difficult to transfect and their behaviour is strongly affected by the exposure to fluorescent light. By examining the appearance and behaviour of cell lines, we found the CNS-derived cell line (CAD cells) (Yanping Qi, 1997) as a complementary system to CPNs. CAD cells are not only strikingly similar to CPNs in displaying a single extended neurite/axon associated with a similar size growth cone but also (Figure 1A) but also bear resemblance in their expression profile of the integrin adhesion receptor subtypes (Table B in Supplementary Figure 2), suggesting similar capabilities in sensing the extracellular matrix.

To investigate where the forces generated by actomyosin contractility inside the growth cone are transmitted to the extracellular environment, we combined traction force microscopy with live fluorescence imaging. CAD cells cultured on laminin (LN)-coated polyacrylamide (PAA) gels with a Young's modulus of 0.4 kPa exerted peak stresses of up to 12 Pa (= 12 pN/μm^2) on their environment (Figure 1B). Force transmission sites located to the base of actin-rich filopodia in the growth cone (Figure 1B). We expected that the sites for force transmission coincide with the localisation of talin and vinculin, both proteins involved in mechanotransduction (Jansen et al., 2017). First attempts to visualise these PC proteins using TIRF microscopy of immunolabelled or GFP-talin expressing CAD cells proved to be difficult, because of low signal to noise or high GFP labelling throughout the growth cone, respectively (Supplementary Figure 1A and B). Adhesion structures at the base of filopodia became readily visible using photoactivatable probes (Figure 1C), because the fractions of the PC proteins that were actively involved in cell-adhesion resided longer at sites of adhesion than inactive fractions that rapidly diffused (Stutchbury et al., 2017). Together these data demonstrate that forces to the substrate that drive the advance growth cones are exerted at the sites of integrin-mediated cell matrix adhesions.

CNS-derived neurons anchor to the ECM predominantly through β1 integrins.

To test the involvement of integrin receptors in axon outgrowth, CAD cells were cultured on glass tissue culture dishes coated with 10 μg/ml of the ECM proteins laminin (LN) or fibronectin (FN), which bind to different types of integrin receptors. Whilst neurites of CAD neurons grew on all tested surfaces (Figure 2A), they were about 30-40% longer on the ECM ligands compared to those on Poly-L-lysine (PLL, Figure 2B). Moreover, in contrast to cells on ECM, a large population of neurons cultured on PLL did not develop neurites, suggesting that ECM-binding integrins promote neurite growth.

To further examine the contribution of integrins towards axon outgrowth, we first examined which types of integrins are expressed by CAD cells. Using FACS analysis, we found predominantly β1 family integrin expression with high levels of α6β1 and intermediate levels of α5β1, which bind laminin and fibronectin, respectively (Supplementary Figure 2). To test the contribution of β1-integrins to CAD neurite outgrowth, we used validated shRNA plasmids specific for the integrin β1 chain (Wang et al., 2011) to downregulate its expression. Neurite outgrowth of CAD cells was highly affected (80% reduced) when we interfered with β1

integrin function, and neurite length was significantly decreased in comparison to transfected control cells (Figure 2C). Taken together, these experiments demonstrated that β1 integrins promote neurite outgrowth.

Talin and FAK, but not vinculin, are essential for axon outgrowth

In non-neuronal cells, talin and vinculin link integrins to the force-generating actomyosin machinery (Atherton et al., 2015; Jansen et al., 2017). To examine whether, and to what extent, these two adapter proteins have a role in axon outgrowth, we performed knockdown experiments using shRNA (Figure 3A and B). Similar to many other cell types, neurons express both members of the talin protein family: talin1 and talin2 (Manso et al., 2017; Monkley et al., 2001). Whilst the knockdown of either talin1 or talin2 had a small effect on neurite outgrowth (reduction from 125 μm to 95 μm over a period of 48 hours in vitro), depletion of both talin proteins together essentially abolished neurite outgrowth in CAD cells (Figure 3A and B), similarly as we observed after β1 integrin knockdown. However, vinculin knockdown had no effect on neurite outgrowth (Figure 3A, B and Figure 4C; for knockdown validation see Supplementary Figure 3).

Whilst talin and vinculin are adapter proteins linking integrins to the actin cytoskeleton (Atherton et al., 2016a; Atherton et al., 2015), FAK is thought to regulate adhesion pathways through its action as a tyrosine kinase (Kleinschmidt and Schlaepfer, 2017). Previously, it was shown that FAK expression is negatively correlated with substrate stiffness (Jiang et al., 2008) and FAK phosphorylation is important for neuronal outgrowth. Here we found that FAK knockdown resulted in an almost complete inhibition of neurite outgrowth (Figure 3A and B). Interestingly, outgrowth inhibition was not related to the kinase function of FAK because application of a specific FAK phosphorylation inhibitor (FAK[i]), which efficiently blocks FAK phosphorylation ((Horton et al., 2016b) and Figure 3E), had no effect on neurite outgrowth (Figure 3C).

These data indicate that talin and FAK but not vinculin are essential for neurite outgrowth. The contribution of FAK to neuronal growth was not mediated by its kinase function, but possibly by its ability to act as a scaffolding protein.

Vinculin regulates neuronal mechanosensing

Having identified a role for PC proteins in transmitting forces generated in the growth cone to the outside world and thus in regulating neurite outgrowth, we next investigated how

CNS-derived neurons respond to different mechanical stimuli. As mechanical interactions will not only depend on cellular forces but also on the mechanical properties of the cells' environment, we cultured CAD cells on FN-coated PAA gels with elastic moduli of 0.4 kPa ('soft') and 8 kPa ('stiff') (Figure 4). Neurite growth significantly depended on substrate stiffness, with ~20% longer processes on soft gels compared to stiff gels (Figure 4A and B), indicating mechanosensing of neurons.

Vinculin has a well-established role in mechanosensing of non-neuronal cells (Atherton et al., 2016a). To examine a potential involvement of vinculin in neuronal mechanosensing, we compared vinculin depleted cells (shRNA) with control cells and analysed neurite outgrowth on soft and stiff substrates. In contrast to the control cells, vinculin-depleted neurons showed no neurite outgrowth-dependence on substrate stiffness. Instead, on both soft and stiff substrates neurites were of similar lengths as control neurons on soft substrates (Figure 4C). These observations suggested a similar mechanosensing role of vinculin in PCs as has been shown for vinculin in FAs for non-neuronal cells (Atherton et al., 2016a; Carisey and Ballestrem, 2011; Carisey et al., 2013a). In line with our earlier observations, shRNA-mediated depletion of β1 integrin or both talin1 and talin2 prevented neurite outgrowth regardless of substrate stiffness (Figure 4C).

In summary, these experiments demonstrated that axon outgrowth of CAD cells on fibronectin and laminin is integrin-mediated, and that vinculin is critical for neuronal mechanosensing.

CPNs respond to ECM and stiffness in a similar manner to CAD cells

CAD cells are a mouse CNS-derived cell line (Qi et al., 1997). We next wanted to explore whether CAD cell mechanosensing mechanisms were also shared with mice cortical primary neurons (CPNs). To explore this we repeated some of the key experiments using CPNs. We found that they readily extended their axons on both laminin and fibronectin (Figure 5A and B). Importantly, CPN axon outgrowth on both LN and FN was blocked when cells were cultured on anti-β1 integrin blocking antibodies, demonstrating that axon outgrowth was mediated by β1 integrins (Figure 5C). CPN axon outgrowth on LN was also reduced when cells were cultured on anti-α2 or anti-α6 blocking antibodies (Supplementary Figure 2A), showing the contribution of these integrin subtypes for axon outgrowth on laminin. FACS analysis using specific antibodies against specific integrin subtypes revealed that CPNs had an integrin profile that was strikingly similar to CAD cells, with high/intermediate levels of α6β1/α5β1 and no β3 integrins (Supplementary Figure 2B, C).

Towards mechanosensing and the potential involvement of vinculin in this process, we found that CPNs extended significantly longer axons when cultured on soft (0.4 kPa) rather than stiff gels (8 kPa, Figure 5D). Importantly, similar to CAD cells, the ability to differentiate substrate stiffness was blocked through the depletion of vinculin using siRNA, which had no overall effect on axon outgrowth (Figure 5E).

In summary, these experiments demonstrate axon outgrowth of cortical neurons on fibronectin and laminin is integrin mediated and that vinculin is critical for neuronal mechanosensing.

Discussion:

In this study we have investigated the role of integrin-associated protein complexes in ECM sensing by CNS-derived neurons. The key findings were that talin and FAK, but not vinculin, are central for axon and neurite outgrowth, and that vinculin is critical for the ability of neurons to discriminate between stiff and soft substrates (mechanosensing).

The role of ECM for axon outgrowth

While the classical ECM integrin ligands LN and FN are not hugely abundant in the brain (Gardiner, 2011), evidence for an important role of ECM in regulating neuronal growth exists from both *in vivo* and *in vitro* data (Plantman, 2013). *In vivo* studies have outlined the significance of LN and other ECM components in the brain with LN being expressed in patterns similar to the distributions of early elongating nerve fibres, thus promoting axonal growth (Letourneau, 1979; Schmid and Anton, 2003; Venstrom and Reichardt, 1993). Our data show that ECM detection via integrins is important, since blocking integrins inhibits axon outgrowth (Figures 2 and 5).

Primary cells and cell lines have similar ECM sensing mechanisms

Primary cells and cell lines may respond very differently to extracellular cues. Therefore, one must carefully evaluate similarities and differences before drawing conclusions when using cell line models. We have tested a variety of CNS-derive cell lines (data not shown) and found that CAD cells were very similar to CPNs. They have a similar morphology with one major neurite growing from the main cell body; they have a very similar growth cone structure and cytoskeletal arrangement; they are similar in their integrin profile (Supplementary Figure 2), and most importantly, they respond to stiffness changes in the same way as primary murine cortical neurons in our experiments (Figure 5). Our data are consistent with previous studies showing that axons of mouse hippocampal neurons (0.5 kPa

vs 4 and 7.5 kPa; (Kostic et al., 2007)) and rat DRG neurons (0.87 vs 13 kPa; (Kostic et al., 2007)) are longer on softer PAA gels. This suggests that all these rodent neuronal cells, primary cells and cell lines, may share similar sensing mechanisms. However, other neuronal cell types may exploit different mechanisms, as for example *Xenopus* retinal ganglion axons grow longer on stiffer substrates (Koser et al., 2016).

The sensory adhesion machinery in PCs and their role for axon/neurite outgrowth.

We have shown that PCs are the sites where growth cones exert forces and sense the ECM (Figure 1). Pathfinding assays suggest that ECM is also instructive (Clark et al., 1993; Kilinc et al., 2015; Li and Folch, 2005) and it will be interesting to investigate to what extent ECM signalling is instructive in more complex signalling environments which are relevant *in vivo*. Indeed, Robles and colleagues showed that local FAK signalling in the growth cone can steer axon outgrowth under the influence of laminin (Robles and Gomez, 2006).

A number of studies, predominantly in non-neuronal cells, showed that integrin-mediated adhesion sites not only serve as cell adhesion focus points, but also as important sites for signalling events (Jansen et al., 2017). FAs are associated with a large network of structural and regulatory proteins that not only serve as mechanosensing devices (Geiger et al., 2009), but also host more than 150 proteins that serve as a platform for a large number of signals that control cell adhesion, protrusion, survival and many more processes (Horton et al., 2016a; Jansen et al., 2017; Kanchanawong et al., 2010; Schiller et al., 2011; Zaidel-Bar et al., 2007). PCs host a similar set of adhesion proteins as FAs, including structural proteins (e.g talin, vinculin) and signalling proteins (e.g. FAK, paxillin and others (C.O. Arregui, 1994; Gomez et al., 1996; Renaudin et al., 1999)). Evidence that these proteins serve not only as passive bystanders comes from reports showing that signalling components such as Src, FAK, paxillin and the associated PAK-PIX pathways regulate adhesion dynamics, axon outgrowth and pathfinding in Xenopus and Zebrafish neurons (Myers and Gomez, 2011; Robles and Gomez, 2006; Vogelezang et al., 2007; Woo et al., 2009). In our experiments, we found that both FAK and talin are critical for neurite outgrowth; depletion of either inhibited axon/neurite outgrowth (Figure 3). However, both protein family members talin1 and talin2 needed to be depleted to achieve the strongest effect (Figure 4A and B), suggesting that one talin protein can at least partially rescue the loss of the other.

Whilst FAK may be required to stabilise lamellipodial protrusions which, through feedback processes, may help generating forces in the growth cone (Moore et al., 2012; Robles and Gomez, 2006), the observed outgrowth inhibition upon talin depletion might be due to a defect in integrin activation (Moser et al., 2009) and subsequently a lack of adhesion and force

transmission (Atherton et al., 2016b; Franze, 2020; Zhang et al., 2008). Knockdown of talin thus abolishes integrin signalling as a whole (Figure 3A and B) and has similar effects as blocking integrins with antibodies (Figure 2C).

Vinculin controls neuronal mechanosensing

Grey matter is stiffer than the white matter in a rat cerebellar tissue and it was hypothesized that this regional heterogeneity influences growth cone guidance (Christ et al., 2010; Franze, 2011; Koser et al., 2016). Also, in disease or injury, changing mechanical signals could play a role in neuron regeneration (Moeendarbary et al., 2017; Murphy et al., 2011). Moreover, we (Figures 4 and 5) and others (Kerstein et al., 2013; Koch et al., 2012; Koser et al., 2016) have shown that neurons can discriminate between soft and stiff substrates. In this study we show that vinculin plays a critical role in the ability of cells to discriminate between soft and stiff environments. Whilst depletion has no effect on axon outgrowth *per se* (in contrast to vinculin knockdown in PC12 cells (Varnum-Finney and Reichardt, 1994)), in cells without vinculin mechanosensing is impaired and cells have the same neurite length on both soft and stiff substrates and is comparable to the soft substrate control (Figures 4C and 5E). Depletion of talin1 or talin2 separately also impaired sensing of substrate stiffness (Figure 4C), and we speculate that this may be due to compromised efficiency of vinculin recruitment to PCs in cells lacking either talin family member. Interestingly, this observation is similar to mechanisms in non-neuronal cells, where knockdown of vinculin leads to cells with normal cell spreading, but they have deficiencies in mechanosensing: fibroblasts without vinculin are deficient in sensing mechanical stimuli and do not repolarise in response to cyclic stretching (Carisey et al., 2013b). Similar results were shown for mesenchymal stem cells, where loss of vinculin inhibited stiffness-driven differentiation (Kuroda et al., 2017; W. et al., 2013), possibly by inhibiting Yap/Taz localization (Kuroda et al., 2017).

Conclusion:

We propose a model whereby integrin-mediated ECM sensing promotes neurite outgrowth. Sensing in PCs of neuronal cells relies on mechanisms similarly present in FAs of non-neuronal cells. Talin is fundamental to couple forces generated by actomyosin to integrins, and without it the adhesion machinery at the base of filopodial protrusions cannot assemble. Signalling proteins such as FAK provide essential cues for cell protrusion, possibly through influencing downstream GTPase activity and actin polymerisation (Moore et al., 2012; Robles and Gomez, 2006). Vinculin is required for mechanosensing and the fine-tuning

of the adhesion machinery, although it is not required for neurite outgrowth per se. Overall, PCs in neuronal growth cones that encounter ECM proteins seem to have similar functions to FAs in non-neuronal cell types, and they are crucial for growth cone motility and mechanosensing.

Materials and Methods

CAD cells

CAD (catecholaminergic-a differentiated) cell line (ECACC catalogue number: 08100805) was established from mouse catecholaminergic neuronal tumours in CNS. CAD cells were maintained in DMEM/FI2 (LZBE12-719F, Lonza) supplemented with 5 mM glutamine, 10% FBS and cultured at 37°C in a 5% CO_2 atmosphere for proliferation. 90% confluent cells were passaged (1:6 split) every 3 days in 10 cm cell culture dishes. To induce differentiation of CAD cells, culture medium was changed to serum-free medium when cells reached 70-80% confluency. After undergoing differentiation for 24 hours, cells were flushed out from culture dishes, collected and then replated in serum-free conditions to re-induce neurite outgrowth within 24 hours.

Isolation of cortical neurons

CPNs were prepared as described previously (Brewer et al., 1993; Lesuisse and Martin, 2002) with minor modifications. In brief, mouse cortices were dissected from the brain tissue of C57/BL6 mice at embryonic days 17.5. Cortices were physically dissociated by repetitive pipetting resulting in a single cell suspension of CPNs. CPNs were plated on substrates coated with ECM proteins including 2 µg/ml of laminin (L2020, Sigma) and 10 µg/ml of fibronectin (P1141, Sigma) or 0.01% of poly-l-lysine (PLL; P4707. Sigma). Cells were cultured in neurobasal medium (21103-049, Life Technologies) supplemented with 5mM glutamine (35050-061, Life Technologies) and 2% B-27 supplement (17504-044, Life Technologies) for 2-5 days *in vitro* (DIV) at 37°C in a 5% CO_2 atmosphere.

Integrin profiling by Fluorescence-Activated Cell Sorting (FACS) analysis

For FACS analysis the following antibodies were used for integrin subunits: α6 (1:100; GoH3, mab13501; R&D systems), α5 (1:100; 5H10.27,553319; BD Pharmingen), α4 (1:100; PS/2, sc-52593; Santa Cruz), α3 (1:100; Ralph 3.2, sc-7019; Santa Cruz), α2 (1:100; Sam.G4, M070-0; emfret Analytics), αv (1:100; Rmv7; a gift from Dr Janet Askari in Martin Humphries lab), β1

(1:100; HMβ1-1, 102201, BioLegend for general pool of β1 integrin), β3 (1:100; 2C9,G2, a gift form Dr Janet Askari) and control rat lgG (1:100; 012-000-003; Jackson lmmunoResearch) and hamster lgG (1:100; MCA2356EL; AbD). Tested cells (10^{5-6}/tube) were washed and suspended in 100 µl of FACS buffer (1% bovine serum albumin (BSA: A9647, Sigma) in phosphate buffered saline (PBS)) containing primary antibodies for 1 hour on ice and then washed with 300 µl of FACS buffer 3 times. Cells were then incubated with secondary antibodies (1:100; RPE conjugated anti-hamster IgG, a gift from Dr Janet Askari; 1:100; Alexa 488 conjugated Donkey anti-mouse and anti-rat IgG, Life Technologies) diluted in FACS buffer for 45 minutes on ice followed by 2 washes with FACS buffer and a final wash with PBS prior to FACS analysis. FACS analysis was carried out on a Cyan ADP (Beckman Coulter) with the help of Mike Jackson (Flow Cytometry Core Facility, University of Manchester). Summit software (Summit V4.3, Beckman) was used for the analysis of the samples.

Fixation and immunofluorescence staining

In order to maintain the cellular structures, particularly growth cones, CAD cells and primary neurons were fixed with prewarmed (37°C) fixation buffer containing 4% paraformaldehyde (PFA; P6148, Sigma), 5mM $MgCl_2$ (M8266. Sigma), 60mM PIPES (P6757, Sigma) and 4% sucrose (S0389, Sigma) in PBS for 30 minutes. A quenching buffer (10 mM glycine in PBS; 410225, Sigma) was added for 5 minutes to prevent autofluorescence from aldehydes. Subsequently, cells were permeabilised with 0.2% Triton X-100 (T8787, Sigma) diluted in quenching buffer for 30 minutes. To reduce unspecific background staining in the immunostaining procedure, cells were treated with 3% BSA in PBS and then incubated with primary antibodies diluted in the staining buffer (1% BSA in PBS) for 45 minutes at room temperature (RT). Thereafter cells were gently washed 3 times (3X 30 minutes) with the staining buffer before incubation with secondary antibodies for 1 hour at RT. Cells were then washed twice (2X 30 minutes) with staining buffer. Finally, 4% PFA was used to post-fix antibodies on cells plated on cell culture dishes, glass bottom dishes (P35G-1.5-20-C, MatTek) or coverslips, which was followed by 3 washes with PBS before imaging.

Primary antibodies used were: fluorescein isothiocyanate (FITC) conjugated anti-tubulin antibody (1:250; DM1A; T9026. Sigma) and anti-tubulin (1:250; YL1/2; MAB1864, Millipore) for staining of MTs; anti-talin (1:200; 8d4, T3287, Sigma), anti-vinculin (1:200; hVIN-1, V9264, Sigma) for talin and vinculin. The following secondary antibodies were used: Dylight 488, 594 or 649 conjugated goat anti-mouse or anti-rat IgGs (1:250; Jackson lmmunoResearch). Texas Red Phalloidin (1:250; T7471, Life Technologies) was used for actin

structures. In some cases the cell nucleus was stained with 4'-6-Diamidino-2-phenylindole (1:250; DAPI).

Functional blocking antibody

The same antibodies as used for FACS analysis were used for integrin blocking assays. Final concentrations for function blocking antibodies in culture medium were 10 μg/ml for α6, α4 integrins and rat IgG and 5 μg/ml for β1, α5, α2, αv integrins and hamster IgG. Function blocking antibodies were added in culture medium 30 minutes after cells were plated on the different substrates and then cultured for 18-24 hours in presence of antibodies.

Plasmids

All previously validated shRNA plasmids (sh β 1, shTalin1, shTalin2, shVinculin and shFAK) (Wang et al., 2011) and GFP fusion tag lentiviral vectors (pG1PZ) were provided by Dr Pengbo Wang (Streuli laboratory; University of Manchester). Photoactivatable GFP (PAGFP)-tagged talin and vinculin constructs were generated as described previously (Stutchbury et al., 2017).

Plasmid DNA transfection and protein knockdown

For transfection, cells were cultured to reach 70-80% confluence (approximately: CAD cells at $1x10^{4-5}/cm^2$ and CPNs at $1x10^6/cm^2$). For each condition 2.5μl of Lipofectamine 2000 was mixed with 125μl of Opti-MEM (31985062, Life Technologies) and incubated at RT for 15 minutes. 1-2 μg of DNA/shRNA plasmids diluted in 125μl of Opti-MEM was added and incubated at RT for a further 20 minutes before adding to the cells in a total volume of 2ml of culture medium in each well of a 6 well plate (Corning). The transfection mixture was added to cells and incubated at 37°C in a 5% CO_2 atmosphere for 4 hours (CAD cells) or for 3 days in culture. CAD cells were replated and cultured for an additional 48 hours in the culture medium and then replated again in serum-free or low serum medium to induce differentiation. CPNs were directly replated. Lipofectamine® RNAiMAX transfection Reagent (13778030, Life Technologies) was used for siRNA-mediated knockdown of proteins. Knockdown was performed according to the manufacture's protocols. After at least 18 hours, a 2nd knockdown procedure was carried out to further reduce the expression levels of the target protein. Cells were then replated and cultured for an additional 48 hours in the culture medium and replated again in serum-free medium to induce 24 hour differentiation, allowing neurites to form and to knockdown the protein of interest before imaging.

FAK inhibition

FAKi inhibitor (AZ13256675, Astra Zeneca) was prepared at different concentrations (1, 3 and 5 μM) in DMEM culture medium. DMSO was used as a control. Differentiated CAD cells were plated on FN-coated 6 well plates and cells were left to attach for 15 min at 37°C. Regular DMEM medium was gently exchanged with DMEM containing FAKi or DMSO and cells were cultured for 24 hours. After FAKi treatment, medium was removed and cells were lysed with ice cold RIPA buffer (150 mM NaCl, 1% NP40, 0.1% SDS, 25mM TBS, pH 7.4) containing protease inhibitor cocktail (1:1000, Sigma). Cells were then scraped off the wells and transferred to labelled centrifuge tubes and left on ice for 30 minutes. Then, samples were centrifuged in a bench centrifuge (Sigma) at 4°C for 30 minutes at maximum speed. The supernatant was then transferred to fresh tubes and kept on ice or at -20°C until further processing.

SDS Page gel electrophoreses and western blotting

Cell lysates mixed with 2x SDS sample buffer and boiled at 95°C for 15 minutes were loaded in a NuPage MOPS Bis-Tris 4-12% gel (Invitrogen) with NuPage MOPS SDS Running Buffer (Invitrogen). After electrophoresis the proteins were transferred on a PDVF membrane (Merck Millipore) using an Invitrogen transfer system. After transfer, the membrane was blocked with 5% BSA for 1 hour, washed with PBS-Tween (PBS-T; 4X 5 min) and incubated with primary antibodies at 4°C overnight with agitation. Primary antibodies used: anti pY397-FAK (1:400; Life Technologies), anti α-Hu-FAK (total FAK; 1:1000; Invitrogen), anti α-tubulin (1:1000; DM1A; Sigma), all prepared in 3% BSA in PBS-T. The membrane was washed 4 times for 5 minutes with PBS-T and incubated with infrared secondary antibodies. Secondary antibodies used were: donkey anti-rabbit IRDye 800 and donkey anti-mouse IRDye 680 (both from LICOR) both diluted 1:5000 in 3% BSA in PBS-T. The membrane was washed 4X 5 minutes with PBS-T prior to visualisation using an infrared Imaging System (LICOR, Oddisey Fc).

ECM-coating of glass surfaces

To examine the influence of ECM proteins on CAD cells and CPNs, cells were plated on ECM protein and PLL coated glass bottom dishes (P35G-1.5-20-C, MatTek; P06-20-1.5-N, In Vitro Scientific). For coating, glass bottomed dishes were incubated with ECM proteins (2 μg/ml of LN, 10 μg/ml of FN) and PLL (0.1 μg/ml) for 1 hour at RT. Thereafter surfaces were washed 3 times with PBS and were kept in PBS prior to use.

460
461
462 **Preparation of PAA gels**
463 Thin layers of PAA gels were prepared according to previous publications with modifications
464 (Pelham and Wang, 1997). Briefly, glass bottom dishes were pre-treated with 0.1N NaOH
465 (Fisher Scientific) then treated for 5 minutes with 3-Aminopropyl trimethoxysilane (APES;
466 A3648, Sigma) to amino-silanise the surface. This was followed by 0.5% glutaraldehyde
467 (G5882, Sigma) treatment for 30 minutes to add functional groups for PAA gel binding (Wang
468 and Pelham, 1998). For sterilisation, dishes were immersed overnight in 70% ethanol (Fisher
469 Scientific). The following procedures were carried out in a tissue culture hood. A range of
470 concentrations of premixes (varying acrylamide concentrations from 3, 5, 6, 10, 15, 20, 25 to
471 30%) was prepared from a 30 % acrylamide solution (EC-890, Protogel, 30 %, 37.5:1 ratio
472 acrylamide/bis-acrylamide solution, National Diagnostics) in PBS. The solution was degassed
473 for 20 minutes. For gelation, final concentrations of 0.1 % (v/v) ammonium persulfate
474 (A3678, Sigma) and 0.01 % (v/v) tetramethylethylenediamine (TEMED; T9281, Sigma) were
475 mixed with PAA premixes. To prepare a thin layer of PAA gel, 8 µl of the gel mixture were
476 added to the glass bottom dishes prepared earlier, and covered by an acid-washed coverslip.
477 After 30 minutes at 37°C, the gel was immersed in PBS for 15-30 minutes; coverslips were
478 then carefully removed and PAA gels were washed 3 times with PBS before use. For ECM-
479 coating of PAA hydrogels the acid-washed glass coverslip covering the PAA gel was pre-
480 coated with 50µg/ml of ECM protein for 1 hour at RT.
481
482 **Elasticity measurement of PAA gels by Atomic Force Microscopy (AFM)**
483 Elasticity measurements were done on 3, 5, 6, 10, 15, 20, 25 and 30% of PAA gel and
484 performed with an AFM (Nanowizard, CellHesion 200; JPK Instruments, Berlin, Germany). For
485 some experiments, tipless AFM cantilevers (Arrow TL1, k = 0.03 N/m; NanoWorld, Neuchâtel,
486 Switzerland) attached to 4.5µm diameter polystyrene beads were used (Novascan, Ames,
487 USA), for others, 10µm diameter polystyrene beads (PPS-10.0, Kisker) were attached to
488 tipless cantilevers (NP-O10, Bruker AFM Probes). Cantilevers were calibrated in medium-
489 filled chambers using the thermal noise method prior to the experiments (Hutter and
490 Bechhoefer, 1993). Each PAA gel was indented 10 to 15 times at 3 random regions with an
491 approach speed of 5 □m/s and a loading force of 5 nN. The obtained force-indentation curves
492 were fitted using built-in JPK software implemented with the Hertz-model for a spherical

indenter, giving the Young's modulus E (Radmacher, 2002). The Poisson ratio of the cells was taken as 0.5.

Traction force microscopy

PAA gel containing 1:100 dilution of 0.2µm FluoSpheres® carboxylate-modified microspheres (F8805, blue fluorescent (365/415); F8811, green fluorescent (505/515); F8810, red fluorescent (580/605), Life Technologies) were prepared using previously published methods with modifications (Koch et al., 2012). Images of fluorescent beads were recorded at 5 or 60 seconds interval on 3i and Delta Vision systems respectively. Images of cells (termed cell image) were captured simultaneously to determine their position. Traction forces exerted by growth cones were measured by analysing the bead displacement over time. In order to obtain the "no forces" reference, cells were treated after time-lapse recordings with 0.05% Triton X-100, which leads to cell detachment and complete relaxation of the PAA gel. The time-lapse images of beads were aligned to correct the shift of each image using Linear Stack Alignment with SIFT (FIJI plugin). Traction stress maps were calculated for each frame with a TFM software package (Han et al., 2015) using MATLAB R2018b. Postprocessing of the data was carried out with a custom Python 3.6 script.

Photoactivation experiments

Photoactivation (PA) experiments were carried out on a spinning disc confocal microscope system (3i) with three phases: (1) pre-activation phase capturing images before probe activation in both the 594nm channel (for LifeAct-RFP construct that labelled actin fibres) and the 488nm channel to image photoactivated fluorescence of the PAGFP-fusion constructs; (2) photoactivation phase where a 405nm laser was pulsed onto a user-defined region of interest (ROI) to activate the probe; (3) post-activation phase captured 60 images in both channels (488nm and 594nm) at 10 second intervals immediately after the PA event for 10 minutes.

Imaging

For measurements of axon outgrowth, neurons were fixed and stained after 24 hours in culture for CAD cells and after 2-5 days in culture for CPNs. For lower magnification imaging we used a Zeiss Axiovert 200M inverted microscope equipped with a motorised X-Y stage (Ludl) and a 20x/0.3 air Ph1 objective. Cytoskeletal and adhesion proteins in fixed cells were visualised with an inverted Delta Vision (Applied Precision, Washington, USA) widefield microscope system equipped with oil-immersion objectives of 40X (NA=1.3), 60X (NA=1.42)

and 100X (NA=1.35) magnification. The microscope was coupled to a CoolSnap HQ charge-coupled device (CCD) camera from Princeton Instruments (Lurgan, UK) and the filter sets were from Chroma Technology (8600v2; Chroma Technology; USA).

Image analysis

For CAD cells, all measurements of neurite length included only measurements of the primary and longest neuronal projection which had at least a length of 30 μm. For CPNs, the axon measured was at least three times longer than the rest of the neurites (Lucci et al., 2020). We only performed measurements in CAD cells or CPNs that showed isolated axons/neurites, to avoid the influence of cell-cell interactions. Image analysis of neuronal outgrowth length was done using manual tracking with the segmented line tool and calculation on FIJI (Schindelin et al., 2012).

Statistics

Neurite/axon length data were presented with box and whisker plots showing median, minimum and maximum value and first and third quartile. Neurite/axon length data were obtained from n=3 independent experiments and pooled together for statistical analysis. Statistical analysis was performed in GraphPad using non-parametric Mann-Whitney test with two-tailed P-value calculation. P value is <0.00001 for ****, <0.0001 for ***, <0.001 for **, <0.01 for * and <0.1 for N.S. (not significant).

Acknowledgements:

This work is supported by the BBSRC, EPSRC, MRC and Wellcome Trust. The C.B. laboratory is part of the Wellcome Trust Centre for Cell Matrix research, University of Manchester, which is supported by core funding from the Wellcome Trust (grant number 088785/Z/09/Z). The authors wish to acknowledge the funding provided by the Biotechnology and Biological Sciences Research Council (BBSRC) to C.M. and K.J. (BB/ M020630/1).

P.A. and A.J.R. are supported by the Hargreaves and Ball Trust and A.J.R. is supported by the Academy of Medical Sciences (AMS-SGCL7).

K.F. is supported by the European Research Council (Consolidator Award 772326) and the Alexander von Humboldt Foundation (Alexander von Humboldt Professorship).

559 ***References:***

560 Athamneh, A.I., and D.M. Suter. 2015. Quantifying mechanical force in axonal growth and
561 guidance. *Frontiers in cellular neuroscience*. 9:359.
562 Atherton, P., F. Lausecker, A. Carisey, A. Gilmore, D. Critchley, I. Barsukov, and C. Ballestrem.
563 2020. Relief of talin autoinhibition triggers a force-independent association with vinculin.
564 *The Journal of cell biology*. 219.
565 Atherton, P., B. Stutchbury, D. Jethwa, and C. Ballestrem. 2016a. Mechanosensitive components of
566 integrin adhesions: Role of vinculin. *Experimental cell research*. 343:21-27.
567 Atherton, P., B. Stutchbury, D. Jethwa, and C. Ballestrem. 2016b. Mechanosensitive components of
568 integrin adhesions: Role of vinculin. *Exp Cell Res*. 343:21-27.
569 Atherton, P., B. Stutchbury, D.Y. Wang, D. Jethwa, R. Tsang, E. Meiler-Rodriguez, P. Wang, N.
570 Bate, R. Zent, I.L. Barsukov, B.T. Goult, D.R. Critchley, and C. Ballestrem. 2015. Vinculin
571 controls talin engagement with the actomyosin machinery. *Nature communications*.
572 6:10038.
573 C.O. Arregui, S.C., and L. McKerracher. 1994. Characterization of Neural Cell Adhesion Sites:
574 Point Contacts Are the Sites of Interaction between lntegrins and the Cytoskeleton in PC12
575 Cells *The Journal of Neuroscience*. 14:6967-6977.
576 Carisey, A., and C. Ballestrem. 2011. Vinculin, an adapter protein in control of cell adhesion
577 signalling. *European journal of cell biology*. 90:157-163.
578 Carisey, A., R. Tsang, A.M. Greiner, N. Nijenhuis, N. Heath, A. Nazgiewicz, R. Kemkemer, B.
579 Derby, J. Spatz, and C. Ballestrem. 2013a. Vinculin regulates the recruitment and release of
580 core focal adhesion proteins in a force-dependent manner. *Current biology : CB*. 23:271-
581 281.
582 Carisey, A., R. Tsang, Alexandra M. Greiner, N. Nijenhuis, N. Heath, A. Nazgiewicz, R.
583 Kemkemer, B. Derby, J. Spatz, and C. Ballestrem. 2013b. Vinculin Regulates the
584 Recruitment and Release of Core Focal Adhesion Proteins in a Force-Dependent Manner.
585 *Current Biology*. 23:271-281.
586 Christ, A.F., K. Franze, H. Gautier, P. Moshayedi, J. Fawcett, R.J.M. Franklin, R.T. Karadottir, and
587 J. Guck. 2010. Mechanical difference between white and gray matter in the rat cerebellum
588 measured by scanning force microscopy. *Journal of Biomechanics*. 43:2986-2992.
589 Clark, P., S. Britland, and P. Connolly. 1993. Growth cone guidance and neuron morphology on
590 micropatterned laminin surfaces. *J Cell Sci*. 105 (Pt 1):203-212.
591 Critchley, D.R. 2004. Cytoskeletal proteins talin and vinculin in integrin-mediated adhesion.
592 *Biochemical Society Transactions* 32:831-836.
593 Franze, K. 2011. Atomic force microscopy and its contribution to understanding the development of
594 the nervous system. *Current Opinion in Genetics & Development*. 21:530-537.
595 Franze, K. 2020. Integrating Chemistry and Mechanics: The Forces Driving Axon Growth. *Annual*
596 *review of cell and developmental biology*. 36:61-83.
597 Gardiner, N.J. 2011. Integrins and the extracellular matrix: key mediators of development and
598 regeneration of the sensory nervous system. *Developmental neurobiology*. 71:1054-1072.
599 Geiger, B., J.P. Spatz, and A.D. Bershadsky. 2009. Environmental sensing through focal adhesions.
600 *Nat Rev Mol Cell Biol*. 10:21-33.
601 Giannone, G., R.M. Mege, and O. Thoumine. 2009. Multi-level molecular clutches in motile cell
602 processes. *Trends Cell Biol*. 19:475-486.
603 Gomez, T.M., F.K. Roche, and P.C. Letourneau. 1996. Chick sensory neuronal growth cones
604 distinguish fibronectin from laminin by making substratum contacts that resemble focal
605 contacts. *Journal of neurobiology*. 29:18-34.
606 Goult, B.T., J. Yan, and M.A. Schwartz. 2018. Talin as a mechanosensitive signaling hub. *The*
607 *Journal of cell biology*. 217:3776-3784.
608 Han, S.J., Y. Oak, A. Groisman, and G. Danuser. 2015. Traction microscopy to identify force
609 modulation in subresolution adhesions. *Nature methods*. 12:653-656.

Horton, E.R., P. Astudillo, M.J. Humphries, and J.D. Humphries. 2016a. Mechanosensitivity of integrin adhesion complexes: role of the consensus adhesome. *Exp Cell Res*. 343:7-13.

Horton, E.R., A. Byron, J.A. Askari, D.H. Ng, A. Millon-Fremillon, J. Robertson, E.J. Koper, N.R. Paul, S. Warwood, D. Knight, J.D. Humphries, and M.J. Humphries. 2015. Definition of a consensus integrin adhesome and its dynamics during adhesion complex assembly and disassembly. *Nat Cell Biol*. 17:1577-1587.

Horton, E.R., J.D. Humphries, B. Stutchbury, G. Jacquemet, C. Ballestrem, S.T. Barry, and M.J. Humphries. 2016b. Modulation of FAK and Src adhesion signaling occurs independently of adhesion complex composition. *J Cell Biol*. 212:349-364.

Hynes, R.O. 2002. Intergrins: Bidirectional, Allosteric Signaling Machines. *Cell*. 110:673-687.

Jansen, K.A., P. Atherton, and C. Ballestrem. 2017. Mechanotransduction at the cell-matrix interface. *Semin Cell Dev Biol*. 71:75-83.

Jiang, F.X., B. Yurke, B.L. Firestein, and N.A. Langrana. 2008. Neurite outgrowth on a DNA crosslinked hydrogel with tunable stiffnesses. *Ann Biomed Eng*. 36:1565-1579.

Kanchanawong, P., G. Shtengel, A.M. Pasapera, E.B. Ramko, M.W. Davidson, H.F. Hess, and C.M. Waterman. 2010. Nanoscale architecture of integrin-based cell adhesions. *Nature*. 468:580-584.

Kerstein, P.C., B.T. Jacques-Fricke, J. Rengifo, B.J. Mogen, J.C. Williams, P.A. Gottlieb, F. Sachs, and T.M. Gomez. 2013. Mechanosensitive TRPC1 channels promote calpain proteolysis of talin to regulate spinal axon outgrowth. *The Journal of neuroscience : the official journal of the Society for Neuroscience*. 33:273-285.

Kerstein, P.C., R.H.t. Nichol, and T.M. Gomez. 2015. Mechanochemical regulation of growth cone motility. *Frontiers in cellular neuroscience*. 9:244.

Kilinc, D., A. Blasiak, and G.U. Lee. 2015. Microtechnologies for studying the role of mechanics in axon growth and guidance. *Front Cell Neurosci*. 9:282.

Kleinschmidt, E.G., and D.D. Schlaepfer. 2017. Focal adhesion kinase signaling in unexpected places. *Curr Opin Cell Biol*. 45:24-30.

Koch, D., W.J. Rosoff, J. Jiang, H.M. Geller, and J.S. Urbach. 2012. Strength in the periphery: growth cone biomechanics and substrate rigidity response in peripheral and central nervous system neurons. *Biophys J*. 102:452-460.

Koser, D.E., A.J. Thompson, S.K. Foster, A. Dwivedy, E.K. Pillai, G.K. Sheridan, H. Svoboda, M. Viana, L.D. Costa, J. Guck, C.E. Holt, and K. Franze. 2016. Mechanosensing is critical for axon growth in the developing brain. *Nature neuroscience*. 19:1592-1598.

Kostic, A., J. Sap, and M.P. Sheetz. 2007. RPTPα is required for rigidity-dependent inhibition of extension and differentiation of hippocampal neurons. *Journal of Cell Science*. 120:3895-3904.

Kuroda, M., H. Wada, Y. Kimura, K. Ueda, and N. Kioka. 2017. Vinculin promotes nuclear localization of TAZ to inhibit ECM stiffness-dependent differentiation into adipocytes. *Journal of Cell Science*. 130:989-1002.

Letourneau, P.C. 1979. Cell-substratum adhesion of neurite growth cones, and its role in neurite elongation. *Experimental Cell Research*. 124:127-138.

Li, N., and A. Folch. 2005. Integration of topographical and biochemical cues by axons during growth on microfabricated 3-D substrates. *Exp Cell Res*. 311:307-316.

Lin, C.H., E.M. Espreafico, M.S. Mooseker, and P. Forscher. 1996. Myosin Drives Retrograde F-Actin Flow in Neuronal Growth Cones. *Neuron*. 16:769-782.

Manso, A.M., H. Okada, F.M. Sakamoto, E. Moreno, S.J. Monkley, R. Li, D.R. Critchley, and R.S. Ross. 2017. Loss of mouse cardiomyocyte talin-1 and talin-2 leads to beta-1 integrin reduction, costameric instability, and dilated cardiomyopathy. *Proc Natl Acad Sci U S A*.

Meili, R., B. Alonso-Latorre, J.C. del Alamo, R.A. Firtel, and J.C. Lasheras. 2010. Myosin II is essential for the spatiotemporal organization of traction forces during cell motility. *Mol Biol Cell*. 21:405-417.

Moeendarbary, E., I.P. Weber, G.K. Sheridan, D.E. Koser, S. Soleman, B. Haenzi, E.J. Bradbury, J. Fawcett, and K. Franze. 2017. The soft mechanical signature of glial scars in the central nervous system. *Nat Commun*. 8:14787.

Monkley, S.J., C.A. Pritchard, and D.R. Critchley. 2001. Analysis of the mammalian talin2 gene TLN2. *Biochem Biophys Res Commun*. 286:880-885.

Moore, D.T., P. Nygren, H. Jo, K. Boesze-Battaglia, J.S. Bennett, and W.F. DeGrado. 2012. Affinity of talin-1 for the beta3-integrin cytosolic domain is modulated by its phospholipid bilayer environment. *Proceedings of the National Academy of Sciences of the United States of America*. 109:793-798.

Moser, M., K.R. Legate, R. Zent, and R. Fassler. 2009. The tail of integrins, talin, and kindlins. *Science*. 324:895-899.

Murphy, M.C., J. Huston, 3rd, C.R. Jack, Jr., K.J. Glaser, A. Manduca, J.P. Felmlee, and R.L. Ehman. 2011. Decreased brain stiffness in Alzheimer's disease determined by magnetic resonance elastography. *Journal of magnetic resonance imaging : JMRI*. 34:494-498.

Myers, J.P., and T.M. Gomez. 2011. Focal adhesion kinase promotes integrin adhesion dynamics necessary for chemotropic turning of nerve growth cones. *The Journal of neuroscience : the official journal of the Society for Neuroscience*. 31:13585-13595.

Myers, J.P., M. Santiago-Medina, and T.M. Gomez. 2011. Regulation of axonal outgrowth and pathfinding by integrin-ECM interactions. *Developmental neurobiology*. 71:901-923.

Navarro, A.I., and B. Rico. 2014. Focal adhesion kinase function in neuronal development. *Current opinion in neurobiology*. 27:89-95.

Paul C. Bridgman, S.D., Clara F. Asnes, Antonella N. Tullio and Robert S. Adelstein. 2001. Myosin IIB Is Required for Growth Cone Motility. *Journal of Neuroscience*. 21:6159-6169

Plantman, S. 2013. Proregenerative properties of ECM molecules. *BioMed research international*. 2013:981695.

Qi, Y., J.K. Wang, M. McMillian, and D.M. Chikaraishi. 1997. Characterization of a CNS cell line, CAD, in which morphological differentiation is initiated by serum deprivation. *The Journal of neuroscience : the official journal of the Society for Neuroscience*. 17:1217-1225.

Renaudin, A., M. Lehmann, J.A. Girault, and L. McKerracher. 1999. Organization of point contacts in neuronal growth cones. *Journal of Neuroscience Research*. 55:458-471.

Robles, E., and T.M. Gomez. 2006. Focal adhesion kinase signaling at sites of integrin-mediated adhesion controls axon pathfinding. *Nature neuroscience*. 9:1274-1283.

Schiller, H.B., C.C. Friedel, C. Boulegue, and R. Fässler. 2011. Quantitative proteomics of the integrin adhesome show a myosin II-dependent recruitment of LIM domain proteins. *EMBO reports*. 12:259-266.

Schindelin, J., I. Arganda-Carreras, E. Frise, V. Kaynig, M. Longair, T. Pietzsch, S. Preibisch, C. Rueden, S. Saalfeld, B. Schmid, J.Y. Tinevez, D.J. White, V. Hartenstein, K. Eliceiri, P. Tomancak, and A. Cardona. 2012. Fiji: an open-source platform for biological-image analysis. *Nature methods*. 9:676-682.

Schmid, R.S., and E.S. Anton. 2003. Role of Integrins in the Development of the Cerebral Cortex. *Cerebral Cortex*. 13:219-224.

Stutchbury, B., P. Atherton, R. Tsang, D.Y. Wang, and C. Ballestrem. 2017. Distinct focal adhesion protein modules control different aspects of mechanotransduction. *Journal of cell science*. 130:1612-1624.

Thompson, A.J., E.K. Pillai, I.B. Dimov, S.K. Foster, C.E. Holt, and K. Franze. 2019. Rapid changes in tissue mechanics regulate cell behaviour in the developing embryonic brain. *Elife*. 8.

Varnum-Finney, B., and L.F. Reichardt. 1994. Vinculin-deficient PC12 cell lines extend unstable lamellipodia and filopodia and have a reduced rate of neurite outgrowth. *J Cell Biol*. 127:1071-1084.

Venstrom, K.A., and L.F. Reichardt. 1993. Extracellular matrix. 2: Role of extracellular matrix molecules and their receptors in the nervous system. *The FASEB Journal*. 7:996-1003.

Vicente-Manzanares, M., X. Ma, R.S. Adelstein, and A.R. Horwitz. 2009. Non-muscle myosin II takes centre stage in cell adhesion and migration. *Nat Rev Mol Cell Biol*. 10:778-790.

Vogelezang, M., U.B. Forster, J. Han, M.H. Ginsberg, and C. ffrench-Constant. 2007. Neurite outgrowth on a fibronectin isoform expressed during peripheral nerve regeneration is mediated by the interaction of paxillin with alpha4beta1 integrins. *BMC Neurosci*. 8:44.

W., H.A., T. Xinyi, V. Deepthi, V.L. G., F. Alexander, C.Y. Suk, Á.J. C., and E.A. J. 2013. In situ mechanotransduction via vinculin regulates stem cell differentiation. *Stem cells*. 31:2467-2477.

Wang, P., C. Ballestrem, and C.H. Streuli. 2011. The C terminus of talin links integrins to cell cycle progression. *The Journal of cell biology*. 195:499-513.

Woo, S., D.J. Rowan, and T.M. Gomez. 2009. Retinotopic Mapping Requires Focal Adhesion Kinase-Mediated Regulation of Growth Cone Adhesion. *The Journal of neuroscience : the official journal of the Society for Neuroscience*. 29:13981-13991.

Yanping Qi, J.K.T.W., Michael McMillian, and Dona M. Chikaraishi. 1997. Characterization of a CNS Cell Line, CAD, in which Morphological Differentiation Is Initiated by Serum Deprivation. *The Journal of Neuroscience*. 17:1217–1225.

Zaidel-Bar, R., S. Itzkovitz, A. Ma'ayan, R. Iyengar, and B. Geiger. 2007. Functional atlas of the integrin adhesome. *Nat Cell Biol*. 9:858-867.

Zhang, X., G. Jiang, Y. Cai, S.J. Monkley, D.R. Critchley, and M.P. Sheetz. 2008. Talin depletion reveals independence of initial cell spreading from integrin activation and traction. *Nature Cell Biology*. 10:1062-1068.

Ziegler, Wolfgang H., Alex R. Gingras, David R. Critchley, and J. Emsley. 2008. Integrin connections to the cytoskeleton through talin and vinculin. *Biochemical Society Transactions*. 36:235.

Figure 1

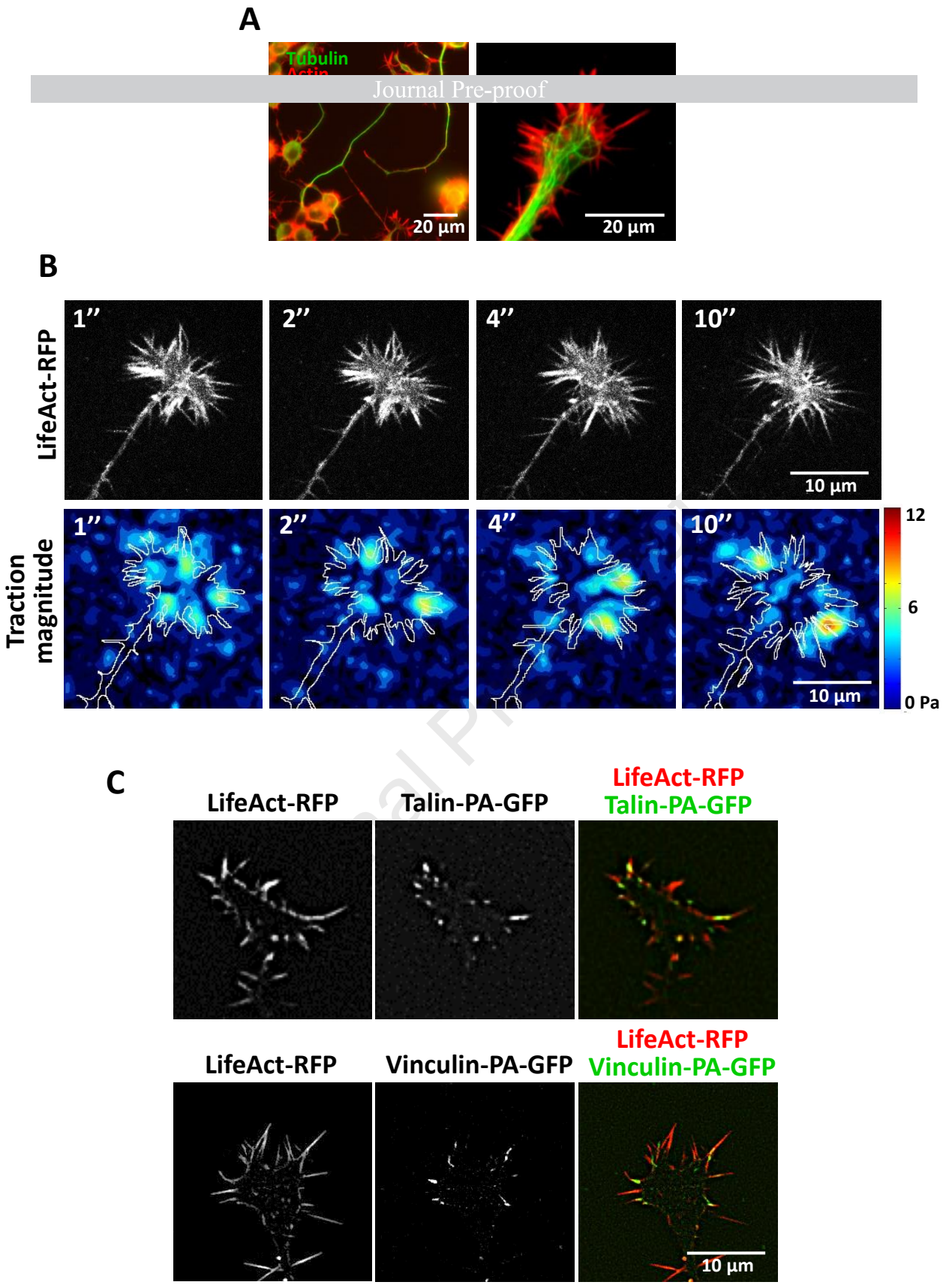

Figure 1. Point contacts (PCs) at the base of base of filopodia of neuronal growth cones transmit forces. Differentiated CAD cells cultured for 24 hours on LN-coated glass **(A)** or LN-coated 0.4 kPa gels **(B,C)** display typical neuronal morphology and growth cones with a peripheral actin-rich zone and dynamic filopodia. **B)** Time-lapse images from traction force microscopy measurements of a growth cone labelled with LifeAct-RFP (top row); force maps (bottom row) colour coded according to force magnitude. Peak stresses located at the base of filopodia range from 5 to 12 Pa. **C)** LifeAct-RFP expressing growth cones co-expressing photoactivatable constructs of talin (PA-GFP-talin) and vinculin (PA-GFP-Vinculin), showing localisation of photo-activated talin/vinculin at the base of the actin-rich filopodia.

Figure 2

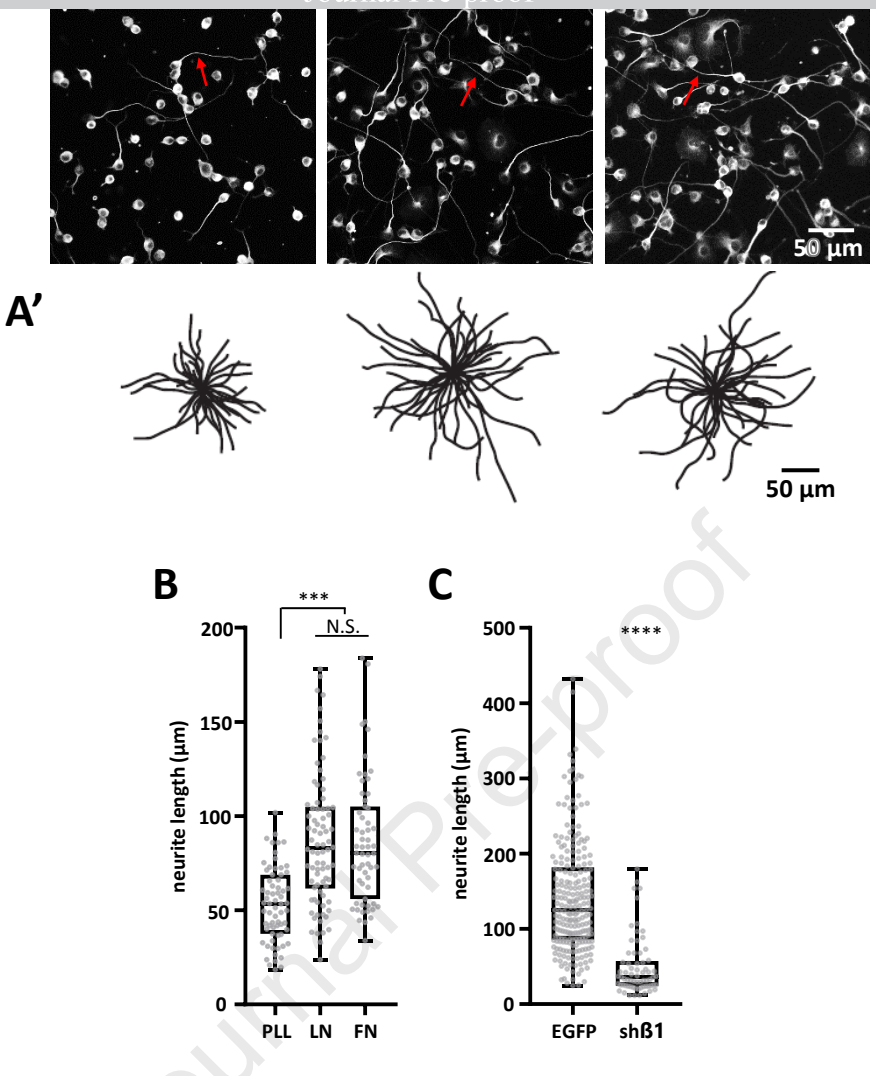

Figure 2. Beta1 integrins promote neurite outgrowth on extracellular matrix. **A-B)** CAD cells were cultured for 24 hours on glass coated with Poly-L-Lysine (PLL), Laminin (LN) or Fibronectin (FN). **A'** Diagrams representing the axonal length and growth trajectories of CAD cells in A, with all neurites aligned to the centre of the diagram. **B)** Measurements of axonal length show that LN and FN promote neurite growth. **C)** CAD cells expressing EGFP shRNA control construct or shRNA specific for the knockdown of the β1 integrin subunit (shβ1). Note the dramatic decrease of the neurite length after β1 integrin knockdown in cells plated for 24 hours on FN. Data in B and C correspond to pooled measurements from n=3 independent experiments. Data presented with box and whisker plots showing median, minimum and maximum value and first and third quartile. Statistical analysis was performed using non-parametric Mann-Whitney test with two-tailed P-value calculation. P value is <0.00001 for ****, <0.0001 for *** significance and <0.1 for N.S. (not significant).

Figure 3

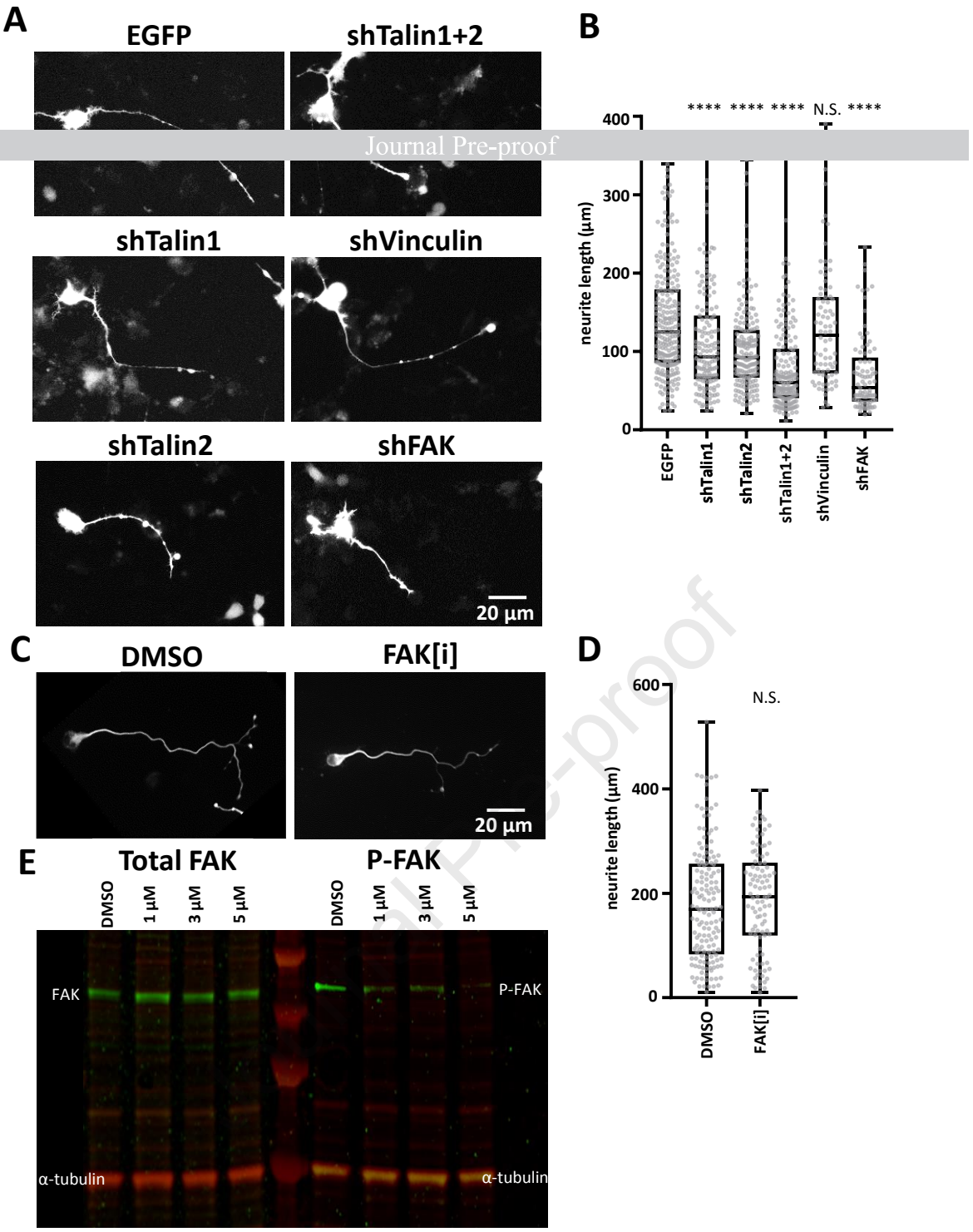

Figure 3. Talin and FAK but not vinculin are required for ECM promoted axon outgrowth. A-B) CAD cells expressing shRNA constructs for the depletion of the indicated proteins. **A)** Tubulin staining was used for labelling of neurites of CAD cells after 24 hours knock down of indicated proteins and a total plated time of 48 hours on FN. **B)** Quantification of neurite length upon depletion of indicated proteins. Note the significantly shorter neurites in cells depleted from talin1, talin2; talin1&2 and FAK in comparison to control cells and vinculin depleted cells. **C)** CAD cells cultured on FN-coated glass and stained for tubulin; cells were treated with DMSO (control) or FAK inhibitor (FAK[i]). **D)** Quantification of neurite length in (C) showing that the inhibition of tyrosine phosphorylation of FAK using FAK[i] does not impair neurite growth. Data in B and D correspond to pooled measurements from n=3 independent experiments. Data presented with box and whisker plots showing median, minimum and maximum value and first and third quartile. Statistical analysis was performed using non-parametric Mann-Whitney test with two-tailed P-value calculation. P value is <0.00001 for **** and <0.1 for N.S. (not significant). **E)** Total FAK (left) and phosphorylated-FAK (Tyr397) (right) protein levels of cell lysates treated with different doses of FAK[i] were visualised by Western blotting together with an α-tubulin control, showing that FAK[i] reduces P-FAK levels efficiently in a dose-dependent manner. Protein ladder used was Precision Plus Protein Standards with visible bands from bottom to top: 50, 75, 100 and 150 kDa.

Figure 4

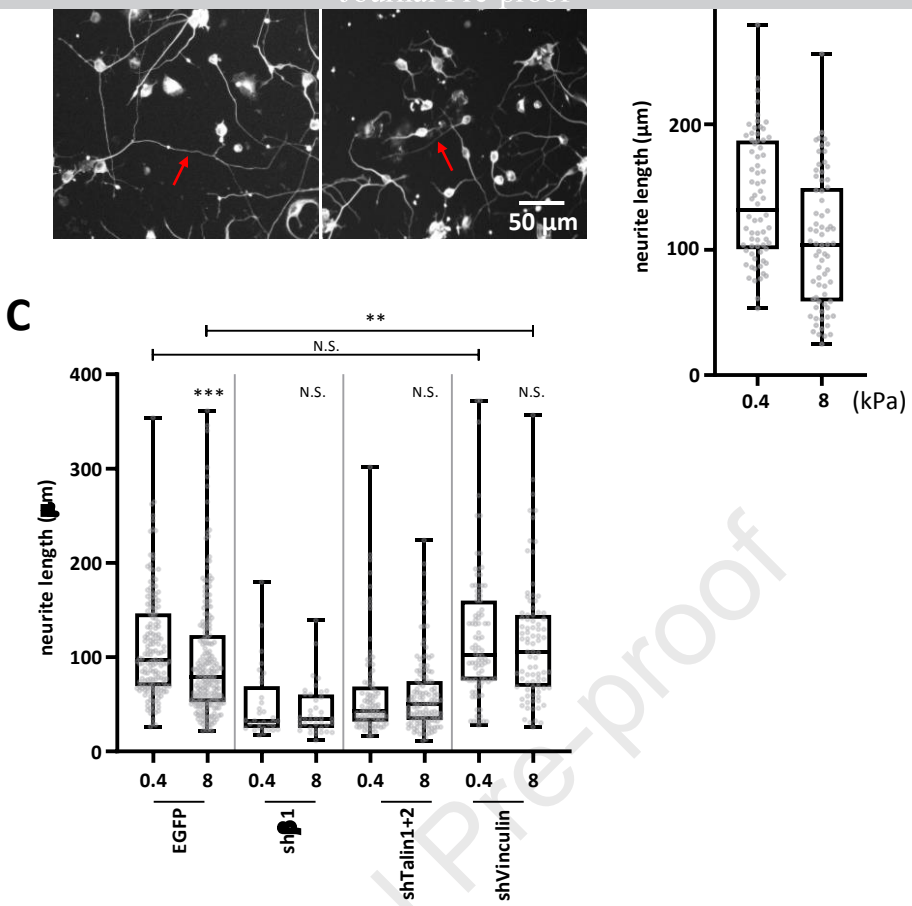

Figure 4. Vinculin mediates mechanosensing in CAD cells. A-C) CAD cells cultured for 24 hours on laminin coated poly-acrylamide gels of indicated stiffness coated with LN. **A)** Tubulin staining was used for labelling of neurites (arrows indicating example neurites) and neurite length was measured. **B)** Quantification of neurite length shows that cells on soft substrates (0.4 kPa) have significantly longer neurites than those on stiff substrates (8 kPa). **C)** Quantification of neurite length of CAD cells expressing indicated shRNA knockdown constructs. Note that depletion of the β1 integrin subunit (shβ1) or the combination of talin1 and talin2 (shTalin1+2) dramatically inhibited neurite outgrowth. In addition, vinculin depletion (shVinculin) did not block neurite outgrowth. Note, however, that neurites of vinculin knockdown cells displayed a similar length on soft and stiff substrates indicating that neurons depleted of vinculin, contrary to control cells, are no longer able to discriminate between soft (0.4 kPa) and stiff (8 kPa) substrates. Data in B and C correspond to pooled measurements from n=3 independent experiments. Data presented with box and whisker plots showing median, minimum and maximum value and first and third quartile. Statistical analysis was performed using non-parametric Mann-Whitney test with two-tailed P-value calculation. P value is <0.00001 for ****, <0.0001 for *** and <0.1 for N.S. (not significant).

Figure 5

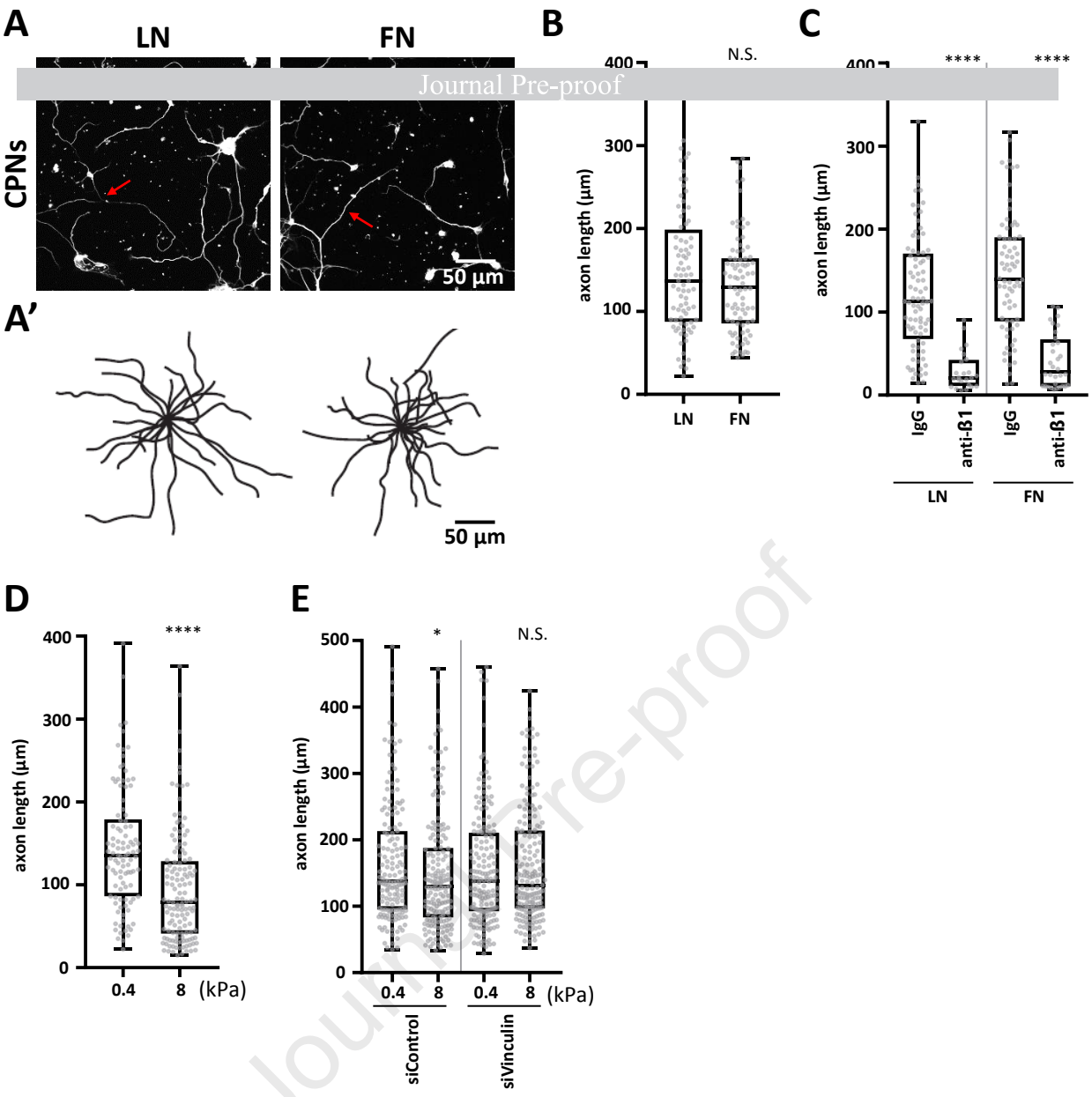

Figure 5. Integrins in CPNs mediate axon outgrowth and vinculin mediates mechanosensing. A-C) Mouse cortical projection neurons (CPN) were cultured for 4 days on glass coated with LN or FN. **A)** CPNs stained for tubulin to measure axonal length. **A',** Diagrams representing the axonal length and growth trajectories of CPNs in A, with all axons aligned to the centre of the diagram. **B)** Quantification of CPN axon length. **C)** Quantified axon length after culture in presence of anti IgG (control) or function blocking anti-integrin β1 antibody. **D)** CPNs cultured on LN-coated hydrogels of indicated stiffness. Note the significantly increased length of axons on softer substrates. **E)** Quantification of neurite outgrowth of CPNs transfected with control or vinculin siRNA (shVinculin). Note that axons of vinculin-depleted neurons are no longer able to sense substrate stiffness and display the same length on soft (0.4 kPa) and stiff (8 kPa) gels. Data in B-E correspond to pooled measurements from n=3 independent experiments for each plot. Data presented with box and whisker plots showing median, minimum and maximum value and first and third quartile. Statistical analysis was performed using non-parametric Mann-Whitney test with two-tailed P-value calculation. P value is <0.00001 for ****, <0.01 for * and <0.1 for N.S. (not significant).

Supplementary Figure 1

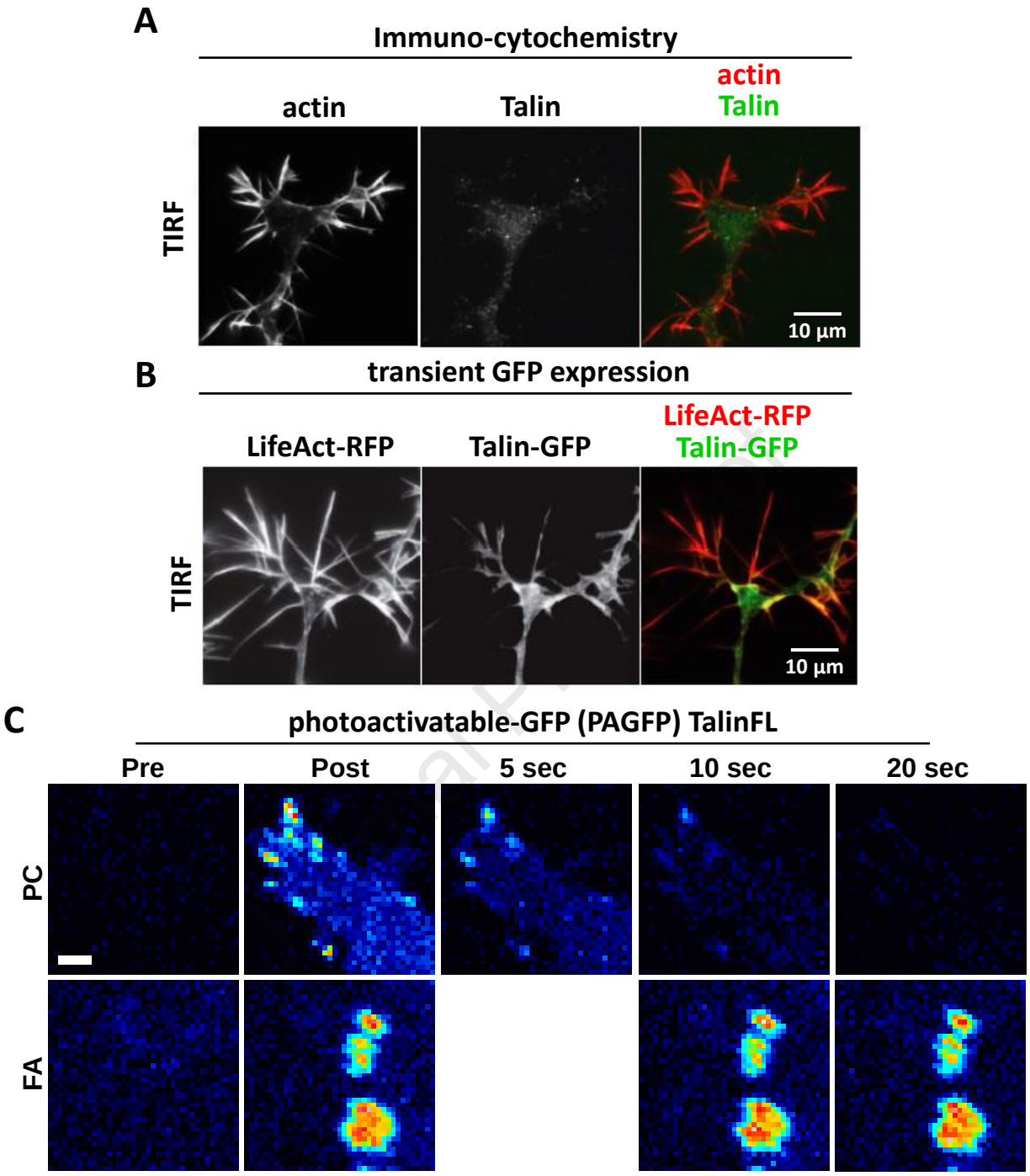

Supplementary Figure 1. Imaging actin and talin in neuronal growth cones.
A) TIRF microscopy of CAD cell growth cones stained for of actin and talin. **B)** TIRF imaging of growth cones of CAD cells expressing LifeAct-RFP and GFP-talin- Compare (A) and (B) with figure 1C for efficiency in adhesion visualisation. Note that only the photoactivatable constructs in figure 1C were efficient in visualising point contacts in growth cones. **C**) Differentiated CAD cells (top panel) or NIH3T3 fibroblasts (lower panel) expressing PAGFP-TalinFL were photoactivated at the growth cone or cell periphery, respectively. Note the dramatic difference in size between point contacts (PC) and focal adhesions (FA) and rate of protein turnover within the two structures; scale bar indicates 2 µm.

Supplementary Figure 2

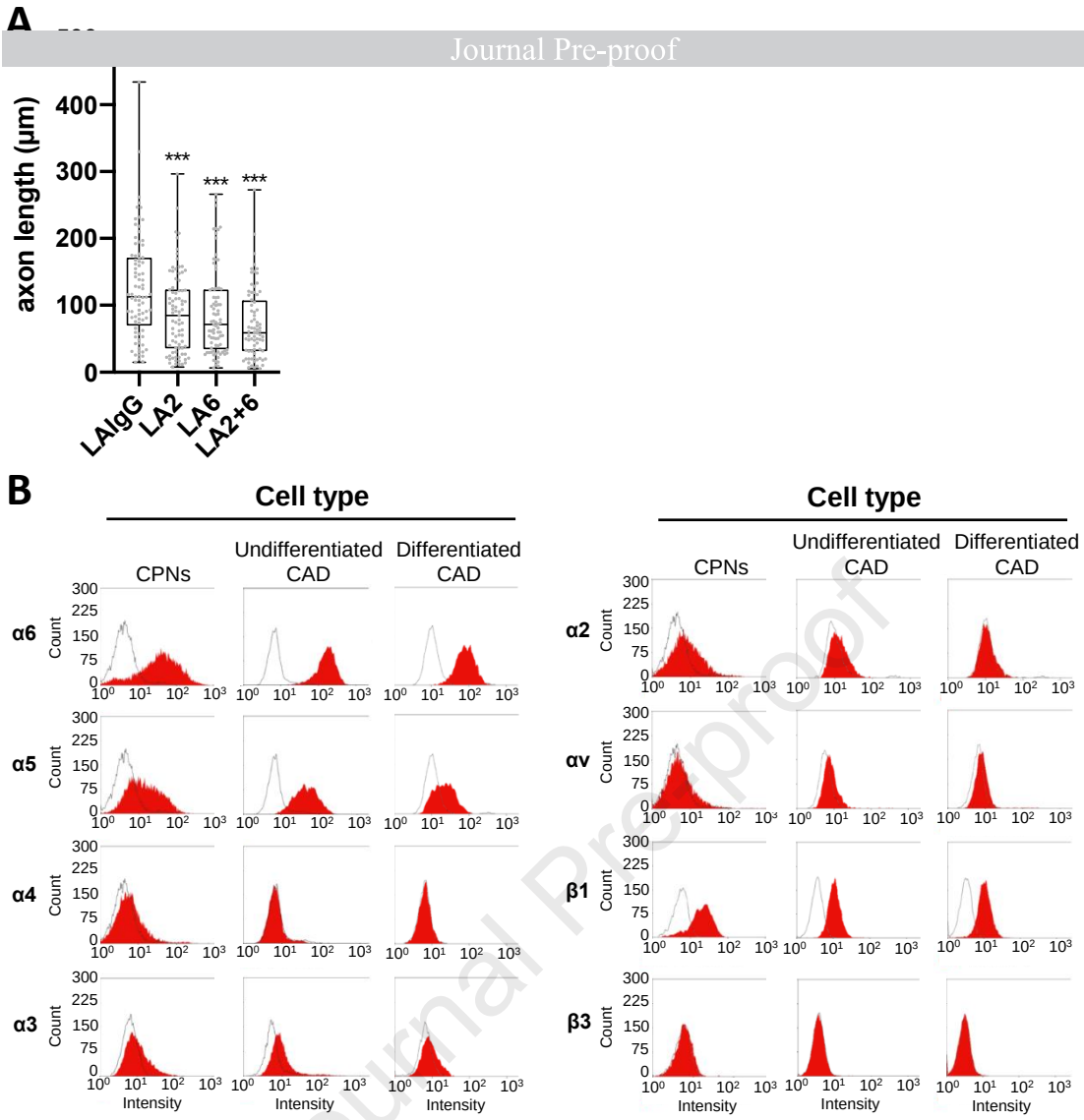

C

Integrin subunit	CPNs	Undifferentiated CAD	Differentiated CAD
α6	++	+++	++
α5	+	++	+
α4	+	-	-
α3	+	+	+
α2	+	+	-
αv	+	+	-
β1	+	+	+
β3	-	-	-

Supplementary Figure 2. Integrin profiles of CAD cells.
A) Mouse cortical projection neurons (CPN) were cultured for 4 days on glass coated with LN. Quantified axon length after culture in presence of anti IgG (control) or function blocking anti-integrin α2 or α6 or α2+α6 antibodies. Data presented with box and whisker plots showing median, minimum and maximum value and first and third quartile. Statistical analysis was performed using non-parametric Mann-Whitney test with two-tailed P-value calculation. P value is <0.001 for ***. **B)** Expression of integrin subunits in neurons was quantified using FACS analysis. Indicated cell types were incubated with antibodies against α6 (GoH3), α5 (5H10.27), α4 (PS/2), α3 (Ralph 3.2), α2 (Sam.G4), αv (Rmv7), β1 (HMβ1-1,), β3 (2C9,G2), and rat IgG (012-000-003) and hamster IgG (MCA2356EL) as control. The black line profile outlines the unspecific control peak while red peaks represent intensity measurements through the binding of anti-integrin antibodies. The higher the shift to the right, the higher the expression level. Histogram is representative for a minimum of two independent experiments with the same outcome. **C)** Table summarising the integrin expression of CAD cells compared to CPNs.

Supplementary Figure 3

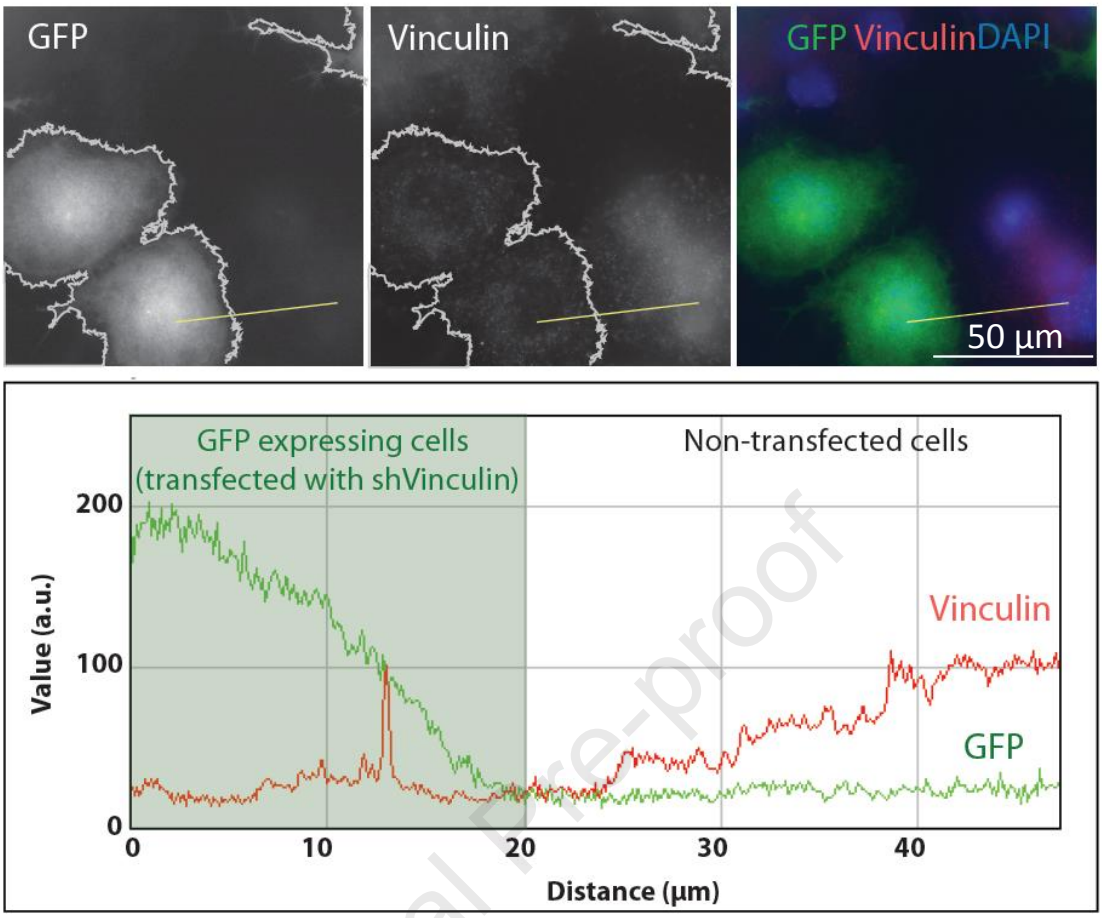

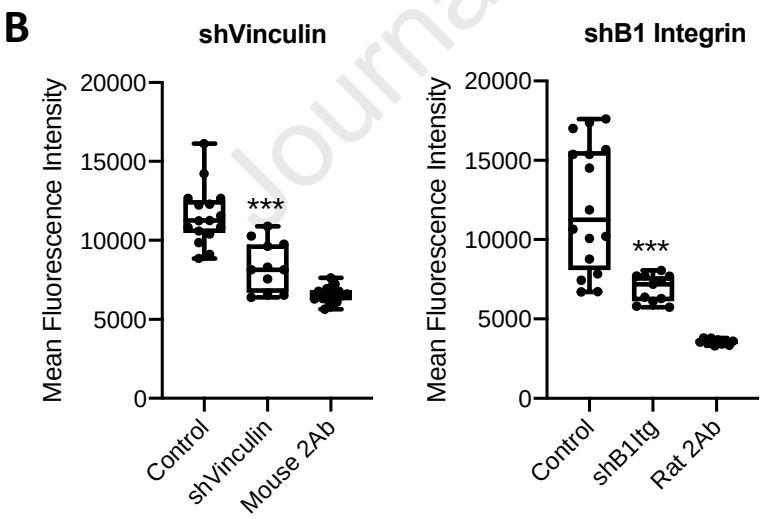

Supplementary Figure 3. Validation of vinculin and β1-integrin knockdown. A) For validation of vinculin knockdown, undifferentiated CAD cells were transfected with published GFP-shVinculin constructs (Wang et al., 2011) for vinculin depletion. Cells were stained for vinculin 72 hours post transfection. Note the decrease of vinculin fluorescence intensities in the cells expressing the GFP-shVinculin in comparison to the neighbouring non-transfected control cells. To visualise this better intensity profiles (lower part of figure) were plotted from line areas displayed in the upper image displays. The nucleus of cells was visualized by DAPI staining. GFP is in green; vinculin in red; and DAPI in blue in the merged images. **B)** Quantification of whole cells fluorescence intensity of undifferentiated CAD cells transfected with Control, GFP-shVinculin or shβ1-integrin constructs, or cells stained with secondary antibody only. *** indicates $p<0.001$, Kruskal-Wallis test.